Competition between electronic and vibrational predissociation dynamics of the $HeBr_2$ and $NeBr_2$ van der Waals molecules

Molly A. Taylor, Jordan M. Pio, Wytze E. van der Veer, and Kenneth C. Janda[a)]
Department of Chemistry and Institute of Surface and Interface Science, University of California, Irvine, California 92697-2025, USA

(Received 12 January 2010; accepted 14 February 2010; published online 11 March 2010)

Direct measurements of the lifetimes of $He^{79}Br_2$ and $Ne^{79}Br_2$ B-state vibrational levels $10 \leq \nu' \leq 20$ have been performed using time-resolved optical pump-probe spectroscopy. The values do not obey the energy gap law for direct vibrational predissociation. For both molecules, the dissociation rate for $\nu'=11$ is much faster than for $\nu'=12$, and the $\nu'=13$ rate is also faster than is consistent with the energy gap law. We attribute this unexpected behavior to an electronic predissociation channel. Based on Franck–Condon factors between the Br_2 B-state vibrational wave functions and the possible Br–Br product wave functions, we surmise that either the Br_2 $^3\Pi_g(1_g)$ or (2_g) state is responsible for the electronic predissociation. To our knowledge, this is the first time electronic predissociation and direct $\Delta\nu=-1$ vibrational predissociation have been observed to be in competition for a wide range of vibrational levels. As such, this problem deserves a detailed theoretical analysis. © *2010 American Institute of Physics*. [doi:10.1063/1.3353954]

I. INTRODUCTION

Ever since the HeI_2 van der Waals (vdW) complex was first observed in a free jet expansion,[1] the photodissocation dynamics of a wide range of rare gas-halogen vdW molecules has been the subject of intense investigation.[2] Early experimental results were indicative of simple dynamics; upon excitation to a vibrational state of the halogen bond, ν', one or more quanta of halogen stretching motion are transferred directly to the rare gas-halogen bond, causing it to break. This process, direct vibrational predissociation (VP), is shown in Eq. (1), where n is the number of quanta transferred to dissociate the rare gas atom (Rg), and X represents a halogen atom.

$$RgX_2(\nu') \rightarrow X_2(\nu'-n) + Rg. \tag{1}$$

The smooth increase in predissociation rate with vibrational quantum number was explained in terms of the energy gap law[3,4] and the equivalent momentum gap law.[5] The basis for this explanation is that the VP rate increases when the wavelength of the product continuum wave function increases and so can achieve better overlap with the initial quasibound vdW wave function multiplied by the coupling. Thus, the rate increases with increasing ν' as the decreasing vibrational energy gap leads to products with less translational energy. For more details, see Fig. 5 of Ref. 2.

The first evidence for more complicated VP dynamics was found for the $ArCl_2$ complex, for which the rotational product state distribution of the Cl_2 product varies dramatically with ν'.[6] Because the $ArCl_2$ complex requires two quanta to break the vdW bond, the initially excited mode couples first to highly excited vdW modes of the $\nu'-1$ manifold of states before dissociating to the $\nu'-2$ continuum.[7] The irregular product state distribution is reflective of these dynamics, which depend strongly on resonances in the flow of energy from the halogen bond to the vdW bond. This process is known as intramolecular vibrational energy redistribution (IVR) and is shown in Eq. (2) for dissociation requiring n quanta of halogen stretching energy.

$$RgX_2(\nu') \rightarrow {}^*RgX_2(\nu'-1) \rightarrow \cdots \rightarrow X_2(\nu'-n) + Rg. \tag{2}$$

In addition to vibrational processes, nonadiabatic electronic predissociation (EP) of the complex is possible if the rare gas atom induces a coupling between the bound halogen electronic state and a dissociative one. The product of EP, therefore, is free halogen atoms, as shown in Eq. (3). In the cases where such a coupling exists, VP and EP are in competition.

$$RgX_2(\nu') \rightarrow 2X + Rg. \tag{3}$$

EP was first observed for ArI_2, and this example is particularly interesting because VP and EP compete for a wide range of ν' levels.[8] The fluorescence excitation spectrum of ArI_2 measured by Kubiak *et al.* shows oscillations in intensity for vibrational levels between 12 and 26.[8] Below $\nu'=12$ no fluorescence is observed. Burke and Klemperer extracted VP probabilities, $k_{VP}/(k_{VP}+k_{EP})$, by measuring both absorption and fluorescence excitation spectra, and they too observed the oscillatory behavior.[9] Unfortunately, the total predissociation rate, $k_{VP}+k_{EP}$, has been measured only for $\nu'=18$ and 21.[10,11] Using these total rates and the VP probabilities from their experiments, Burke and Klemperer were able to extract k_{VP} for those two levels.[9] Then, by assuming a smooth variation in VP rate between the two points, they calculated the EP and VP rates for all the other levels. Three-dimensional wavepacket studies of EP due to Ar-induced coupling to the $a\ ^3\Pi_g(1_g)$ state reproduced the trend in EP rate reported by Burke and Klemperer.[12]

a)Electronic mail: kcjanda@uci.edu.

For ArI_2 three quanta are required to dissociate the vdW bond. Calculations predict that IVR is in the sparse regime, and that oscillations due to IVR are larger than those from EP.[13–15] Burke and Klemperer found that the trend in EP efficiency is qualitatively the same when there is initial vdW excitation, which suggests that the oscillations in intensity are not from coincidental resonances in the sparse IVR regime.[9] Recent measurements of the product rotational state distribution of ArI_2 by the Heaven group failed to provide conclusive experimental evidence that IVR is in the sparse regime.[16] Despite three decades of research, a detailed picture of the dynamics of ArI_2 remains elusive.

More commonly, either EP or VP dominates the dynamics. For complexes of krypton and xenon with I_2, EP occurs on a much faster timescale than VP so that no I_2 product is observed.[17] For the $HeCl_2$ (Refs. 18 and 19) and $NeCl_2$ (Refs. 20 and 21) complexes, the dynamics obey the energy gap law for a wide range of levels, but EP appears to "turn on" for higher levels, and VP products can no longer be observed. For $NeCl_2$, the onset of EP occurs very close to the closing of the $v'-1$ channel, and this led to the hypothesis that EP is related to the onset of IVR.[22] $ArCl_2$ undergoes IVR dynamics for $8 \leq v' \leq 12$, but EP dominates as soon as it becomes energetically possible to form ground state chlorine atoms.[6] A recent attempt to perform *ab initio* calculations to model the competition between EP and IVR dynamics for the $ArCl_2$ and $NeCl_2$ complexes failed to quantitatively reproduce experimental results.[20]

An ideal system for studying electronically nonadiabatic processes in vdW complexes would be one where EP competes with direct VP rather than IVR, so that the EP dynamics could be easily distinguished from the smooth direct VP trend. This would also make theoretical studies much more feasible, since direct VP is mainly sensitive to the repulsive wall of the intermolecular potential, whereas IVR is sensitive to the whole potential.[23]

Direct VP, as opposed to IVR, is expected for systems where the vdW bond energy is small enough so that the $\Delta v' = -1$ channels are open and no intermediate resonances play a role. The $HeBr_2$ and $NeBr_2$ vdW complexes meet this criterion for a wide range of vibrational levels, and many Br_2 dissociative states cross the *B*-state curve over the energy region of these v' levels.

In this paper we present the first real-time measurements of predissociation lifetimes from the $v' = 10$ to 20 vibrational levels of the *B* electronic state of the $He^{79}Br_2$ and $Ne^{79}Br_2$ vdW complexes, and we show evidence for competition between EP and direct VP. While lifetimes have been measured for several of these levels before, the presence of a competing EP pathway was not noticed because, by chance, the levels for which EP is most important were not studied.

II. EXPERIMENTAL SECTION

To create the $HeBr_2$ complexes, helium gas (≈200 psig) is passed over Br_2 held at −16 °C in a stainless steel trap. For the $NeBr_2$ complexes, a 50:50 He:Ne mixture (≈200 psig) is used. The gas mixture is expanded through a 150 μm diameter pulsed nozzle into the vacuum chamber held at approximately 10^{-6} Torr. Rapid cooling of the mixture results in the formation of the complexes, which are studied using pump-probe spectroscopy. In all experiments the $^{79}Br_2$ isotopomer was selected spectroscopically.

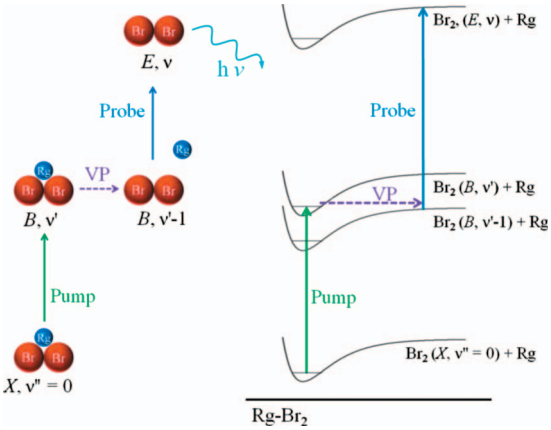

FIG. 1. Illustration of the pump-probe scheme used in the experiments. Details are given in the text.

The tunable laser pulses used in our pump-probe experiments are generated using two optical parametric oscillator-optical parametric amplifiers pumped by a single mode-locked neodymium doped yttrium aluminum garnet laser.[24] This laser system has been described in detail elsewhere.[25] The pulses, which have temporal and frequency resolution of 35 ps and 2 cm^{-1} (full width at half maximum), respectively are tunable between 2 μm and 250 nm. The pump beam is sent through a delay stage before both beams are directed collinearly into a vacuum chamber where they intersect the free jet. The fluorescence signal is monitored using a photomultiplier tube.

The dynamics of the complexes are studied using the pump-probe scheme illustrated in Fig. 1. The Rg–Br_2 potential energy surfaces are shown for states with different numbers of vibrational quanta along the Br_2 coordinate. The pump laser excites the Br_2 moiety within the complex to a vibrational level, v', of the *B* electronic state. During the VP process, vibrational energy from the Br–Br stretch is transferred to the vdW bond, dissociating the rare gas atom and leaving free Br_2 in a lower vibrational level.

The probe laser detects the Br_2 product by exciting it to a vibrational level of the *E* electronic state from which the fluorescence is collected. To prevent saturation of the probe transition, neutral density filters are used to attenuate the beam. Predissociation lifetimes are measured by varying the delay between the pump and probe using the delay stage.

The Rg–Br_2 complexes studied here are the T-shaped complexes. However, both He– and Ne–Br_2 can also form linear isomers with $B \leftarrow X$ spectra that are broad continua lying under the discrete T-shaped transitions.[26,27] Therefore, the T-shaped isomer delay scans have some contamination due to the ultrafast direct dissociation of the linear isomer. The effect of the linear isomer on the fitted lifetimes was tested by subtracting off the linear isomer contribution to the delay scans. The effect was negligible due to the much greater intensity of the T-shaped discrete transitions com-

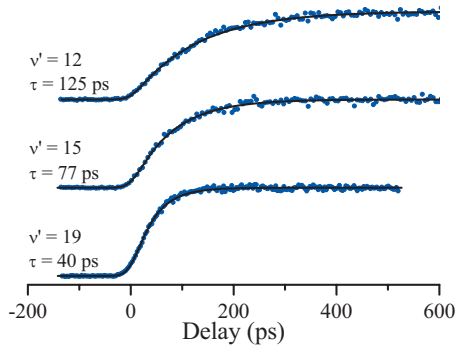

FIG. 2. Data (dots) and fits (lines) for the formation of Br_2 $(B,\nu'-1)$ after excitation of $HeBr_2$ (B,ν').

pared to the broad linear isomer continuum, so all the fits were performed on delay scans without any subtraction of the linear isomer component.

To assure consistency, most lifetimes were measured on at least two separate occasions. To provide an example of the level of signal-to-noise achieved, individual traces with fits are shown for He– and Ne–Br_2 in Figs. 2 and 3, respectively. The lifetime for each initial vibrational level is determined by fitting the data to the convolution of the Gaussian laser cross-correlation with a single exponential rise. Error bars, which are 95% confidence intervals, are assigned using a numerical method described previously.[28] We have slightly modified the procedure to account for the possibility of a ± 4 ps error in the full width at half maximum of the laser cross-correlation. This is particularly important in the present experiment because many of the lifetimes are close to or less than the cross-correlation.

III. RESULTS AND DISCUSSION

Predissociation lifetimes from ν' vibrational levels of the B electronic state of the He– and Ne–Br_2 complexes were measured. The measured lifetimes, which range from 29 to 312 ps, are reported in Table I and Fig. 4. We were surprised to observe that the relationship between the measured lifetimes and ν' is not monotonic for either molecule, and considerable extra data was gathered to confirm the measured error bars and ensure that the results are reproducible. For both complexes the results for $\nu'=11$ are particularly striking, since this level clearly decays faster than does the $\nu'=12$ level. This was the first indication that there is another dissociation channel in competition with VP. In what follows, we describe how we extracted the rates of EP and identified the possible product channel from our data, concentrating on the $NeBr_2$ cluster for which the effect is largest. Then, we discuss the new results in the context of previous work.

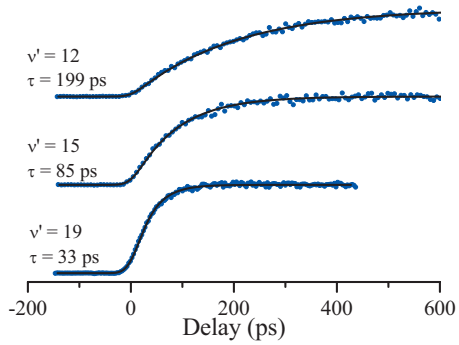

FIG. 3. Data (dots) and fits (lines) for the formation of Br_2 $(B,\nu'-1)$ after excitation of $NeBr_2$ (B,ν').

TABLE I. Predissociation lifetimes for vibrational levels of the B electronic state of $NeBr_2$ and $HeBr_2$.

	$NeBr_2$	$HeBr_2$
ν'	τ (ps)	τ (ps)
10	312 ± 13	157 ± 12
11	114 ± 4	102 ± 6
12	200 ± 4	121 ± 3
13	111 ± 4	81 ± 3
14	94 ± 4	84 ± 3
15	93 ± 3	74 ± 3
16	68 ± 3	59 ± 4
17	49 ± 3	51 ± 3
18	42 ± 2	46 ± 3
19	35 ± 3	39 ± 2
20	29 ± 4	34 ± 3

For the vibrational levels of interest $(10\leq\nu'\leq20)$, the relevant VP process for He– and Ne–Br_2 is $\Delta\nu'=-1$ VP, since one quantum of bromine stretch is enough to break the vdW bond. The B-state binding energies for $NeBr_2$ and $HeBr_2$ are approximately 63 (Ref. 29) and 13 cm^{-1} (Refs. 30 and 26), respectively, which corresponds to a $\Delta\nu'=-1$ channel closing above $\nu'=27$ for $NeBr_2$ (Refs. 29 and 31) and $\nu'=45$ for $HeBr_2$.[30] We confirmed that for the $\nu'=15$ and 20 levels of $NeBr_2$ the $\Delta\nu'=-2$ process accounts for only about 5% and 13% of the VP products, respectively. This is in good agreement with quantum dynamics calculations, where for $\nu'=20$ approximately 12% of the VP products undergo $\Delta\nu'=-2$ dissociation.[32]

Although IVR is possible for $\Delta\nu'=-1$ VP, it would require that energy in excess of the binding energy be transferred to rotation of the complex supported by a centrifugal barrier.[32] The vibrational spacings for the $\nu'=10$ and 15 levels of $^{79}Br_2$ are 132 and 112 cm^{-1}, respectively.[33] For the more strongly bound $Ne^{79}Br_2$ complex, this corresponds to between 69 and 49 cm^{-1} of excess energy. Measurements of

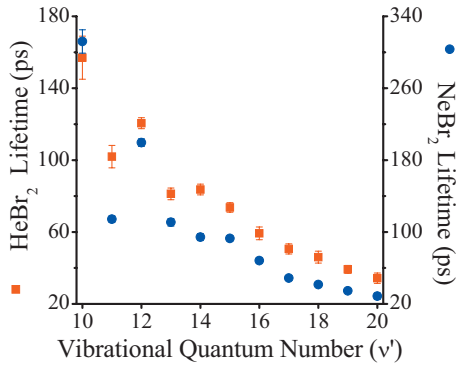

FIG. 4. Predissociation lifetimes for vibrational levels of the B electronic state of $NeBr_2$ (blue circles) and $HeBr_2$ (red squares).

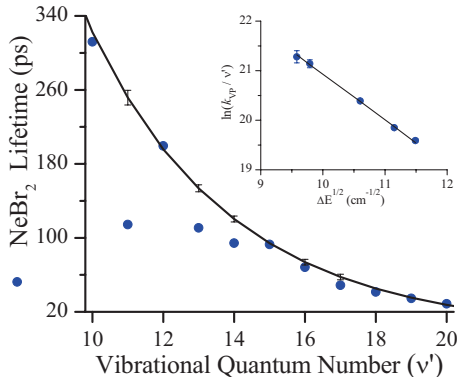

FIG. 5. The energy gap law fit of $\nu'=10$, 12, 15, 19, and 20 used to estimate VP rates for $NeBr_2$. Error bars for the fit are shown for some vibrational levels. The inset shows that a plot of $\ln(\Gamma/\nu')$ vs $\Delta E^{1/2}$ is linear for our data. Error bars are shown for the measured values used in the weighted fit.

the rotational distributions show that for these two levels the average product rotational energies are 5.1 and 5.4 cm^{-1} (7.5 and 11% of the excess energy), and only a small fraction of the products are found in rotational states near the energetic limit.[29] This provides good evidence that IVR dynamics plays at most a small role for the vibrational levels of interest.

Because direct VP most likely dominates the dynamics, the trend in VP rate is expected to obey the energy gap law. However, if a competing EP pathway exists for an initially excited level, ν', the measured rate constant is not simply k_{VP}, but $k_{VP}+k_{EP}$. The corresponding lifetime is $(k_{VP}+k_{EP})^{-1}$. Therefore, if a competing EP channel were present it would show up as an unexpectedly fast lifetime, consistent with what we observe for $\nu'=11$ and 13 (Fig. 4). Two observations support our conclusion that the deviation from the energy gap law is due to EP. First, the measured rates vary nonmonotonically, which is consistent with the oscillatory behavior for Franck–Condon factors between two electronic states. Second, the same levels are affected for both complexes, which is consistent with a process controlled by the electronic structure of Br_2.

Since the EP process is in competition with direct VP and not IVR we assume that the VP rate varies according to the energy gap law, which is shown in Eq. (4).[3] We extracted the VP rates for all the ν' levels by fitting the lifetimes of the longest lived levels to Eq. (4) and interpolating the fit to give the VP rate for the short-lived levels. Therefore, the main assumption in our analysis is that we have identified vibrational levels for which there is no contribution from EP.

$$k_{VP} = A\nu' e^{-(B\Delta E)^{1/2}}. \tag{4}$$

In Eq. (4), ΔE is the energy spacing between adjacent vibrational levels of the Br_2 molecule,[34] and A and B are fitted constants.[35] The data was plotted as $\ln(k_{VP}/\nu')$ versus $\Delta E^{1/2}$, and a weighted linear least-squared fit was performed, with the weighting coefficient equal to one over the variance of $\ln(k_{VP}/\nu')$. The variances were estimated from the variances on the measured rates using a Taylor series expansion.

Figure 5 shows the fit to the $NeBr_2$ data (levels $\nu'=10$, 12, 15, 19, and 20 were fit) in both the linear form and the exponential form. Using the fit, we extracted VP rate constants for each vibrational level. The EP rate constants were then easily determined by subtracting the VP rates from the measured rates. The EP and VP rate constants and EP probabilities $[k_{EP}/(k_{VP}+k_{EP})]$ of $NeBr_2$ are shown in Table II. Error bars on the final EP rates and probabilities were also calculated using the linear approximation. Note that points lying slightly above the fit will yield small negative EP rate constants. To within the error bars, the rate constants are zero. Also, the relative error bars get larger with increasing ν' as the lifetimes get shorter than the laser cross-correlation.

TABLE II. EP rates, VP rates and EP probabilities for vibrational levels of the B electronic state of $NeBr_2$.

ν'	k_{EP} (10^8 s^{-1})	k_{VP} (10^8 s^{-1})	% EP[a]
10	1 ± 2	31 ± 1	3 ± 6
11	48 ± 3	40 ± 1	55 ± 4
12	-1 ± 2	51 ± 1	-2 ± 3
13	25 ± 4	65 ± 2	28 ± 4
14	23 ± 5	83 ± 2	22 ± 5
15	2 ± 5	106 ± 4	1 ± 5
16	11 ± 9	136 ± 6	7 ± 6
17	32 ± 15	173 ± 9	15 ± 7
18	20 ± 19	221 ± 14	8 ± 8
19	6 ± 31	283 ± 21	2 ± 11
20	-14 ± 53	363 ± 31	-4 ± 15

[a]% EP is defined as $[k_{EP}/(k_{VP}+k_{EP})]\times100\%$.

An analogous fit to the $HeBr_2$ data (all points except $\nu'=11$ and 13) is illustrated in Fig. 6. In this case, only for $\nu'=11$ and 13, where the deviations are very large, can separate k_{EP} and k_{VP} components be extracted due to the larger error bars on the $HeBr_2$ data. For $\nu'=11$ $k_{EP}=27(6)\times10^8$ s^{-1} and $k_{VP}=71(2)\times10^8$ s^{-1}, and for $\nu'=13$ $k_{EP}=23(5)\times10^8$ s^{-1} and $k_{VP}=100(2)\times10^8$ s^{-1}.

The fact that the largest deviation from monotonic behavior occurs for the same vibrational levels of $NeBr_2$ and $HeBr_2$ ($\nu'=11$ and 13) suggests that, while the coupling is induced by the rare gas atom, the dominant variable must be the Franck–Condon factors between the bound and free state Br_2 wave functions. Thus, we calculated the Franck–Condon overlap between the ν' wave function of the B electronic

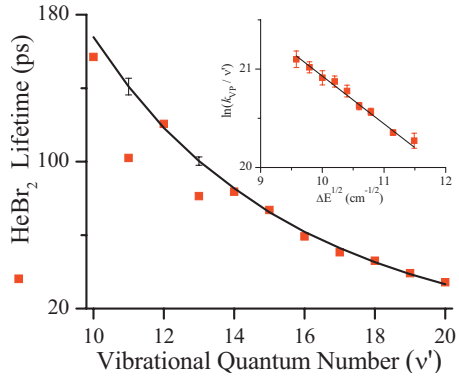

FIG. 6. The energy gap law fit of all points except $\nu'=11$ and 13 used to estimate VP rates for $HeBr_2$. Error bars for the fit are shown for some vibrational levels. The inset shows that a plot of $\ln(\Gamma/\nu')$ vs $\Delta E^{1/2}$ is linear. Error bars are shown for the measured values used in the weighted fit.

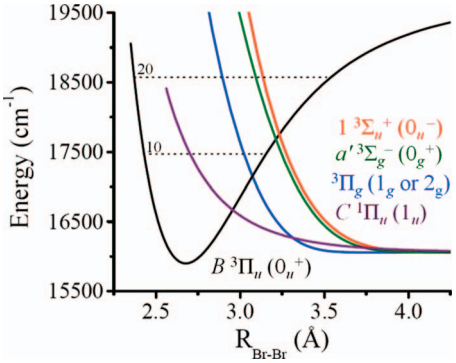

FIG. 7. Br_2 potential energy surfaces used in the calculation of the Franck–Condon factors. The dashed lines indicate the location of the $\nu'=10$ and 20 levels of the B state.

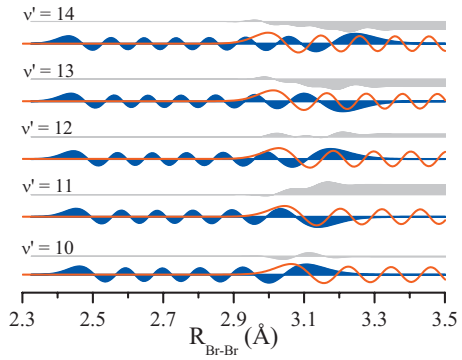

FIG. 9. Franck–Condon overlap between the B-state (blue) and the $1_g/2_g$ state wave functions (red). The vibrational wave function overlap integral (gray) is plotted above each set of wave functions. The square of the value at large R_{Br-Br} is the Franck–Condon factor. See text for more details.

state of $^{79}Br_2$ and the isoenergetic product wave function for the repulsive electronic states that cross the B state. We assume the effect of the rare gas atom is simply to couple the electronic states, i.e., the rare gas atom acts as a spectator. Our analysis neglects any effect of the rare gas atom on the shape of the potential surfaces of Br_2.

The Rydberg–Klein–Rees potential of Barrow *et al.* was used for the B state.[33] The dissociative potentials used, in order of increasing energy, were the $C\,^1\Pi_u(1_u)$ state (Refs. 36 and 37), $^3\Pi_g(2_g)$, $a\,^3\Pi_g(1_g)$, $a'\,^3\Sigma_g^-(0_g^+)$, and $1\,^3\Sigma_u^+(0_u^-)$.[38,39] The $^3\Pi_g(1_g)$ and (2_g) states are almost directly on top of each other, so we are not able to distinguish between them. The potential energy surfaces of the electronic states used to calculate the Franck–Condon factors are shown in Fig. 7. The $^{79}Br_2$ B-state wave functions and dissociative state continuum wave functions were calculated by numerically solving the one-dimensional Schrödinger equation using a discrete variable method.[40] The grid spacing was 0.006 Å. For the B state, the final point on the grid, R_{max}, was at 6 Å. A grid extending to 20 Å was used for the continuum states, safely beyond the distance for which the Franck–Condon factors become independent of R_{max}.

In Fig. 8 the $NeBr_2$ EP rate constants are compared to the corresponding Franck–Condon factors for the potentials shown in Fig. 7. The measured EP rates and error bars are represented in gray, and the Franck–Condon factors are represented in the same color used to illustrate the corresponding potential in Fig. 7. Of the dissociative electronic states we considered, the $^3\Pi_g(1_g)$ and (2_g) states (hereafter referred to as the $1_g/2_g$ state) yield large Franck–Condon factors for the vibrational levels with anomalously fast lifetimes ($\nu'=11$, 13, and 14), and the oscillations in the EP rate closely match the oscillating $1_g/2_g$ Franck–Condon factors over the entire range of ν', although for higher levels the error bars are large. The Franck–Condon factors for the C state vary smoothly with ν', and would not cause oscillations in the lifetime, but would increase the predissocation rate for all levels. So, this analysis is not able to eliminate the possibility of coupling between the B and C states. However, the evidence for coupling between the B and $1_g/2_g$ states is very strong.

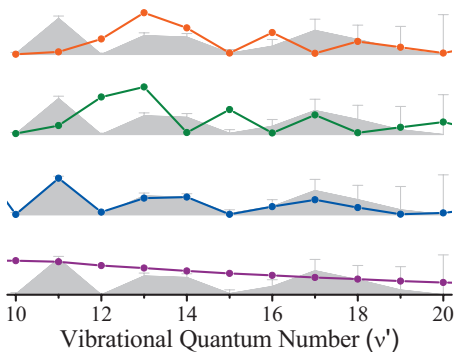

FIG. 8. Estimated EP rate constants (gray) and Franck–Condon factors between the B electronic state and relevant dissociative states (colored and ordered to match the potentials in Fig. 7). The values have been scaled for ease of comparison.

In Fig. 9 the B-state wave functions (blue) and the $1_g/2_g$ wave functions (red) have been plotted along with the vibrational wave function overlap integral (gray), $F(R)=\int_0^R dr'\,\psi_{\nu'}(r')\psi_\epsilon(r')$, for levels between 10 and 14. The value of the integral at large R_{Br-Br} is the square root of the Franck–Condon factor. Because the coupling we have identified here is unusual in that it both oscillates and extends over a long range of vibrational levels, Fig. 9 provides a more detailed analysis of the Franck–Condon factors between the ν' levels of the Br_2 B-state and product functions on the $1_g/2_g$ curves. For $\nu'=10$ the first oscillation of the product wave is almost perfectly out of phase with the outer turning point of the bound state wave function. In contrast, for $\nu'=11$ the overlapping waves are almost perfectly in phase. This trend continues for the higher ν' levels. Our calculations of the Franck–Condon factors also suggest that for $\nu'=8$ and 9 EP will effectively compete with VP. Unfortunately, the small Franck–Condon factors for excitation from the X state result in very weak spectra for these levels, and we have been unable to perform measurements to confirm this prediction. The lifetime of $HeBr_2$ has previously been measured for $\nu'=8$ by linewidth analysis.[41] The resulting value of 150 ps is faster than what we measured for $\nu'=10$ (157 ps) and is much faster than the direct VP rate predicted by the energy gap law fit to our data (256 ps).

To our knowledge, the He– and Ne–Br_2 molecules are the first for which EP dynamics has been observed to be in competition with direct VP. It is even more interesting that the competition extends over a wide range of energy levels.

Our analysis here depends on the assumption that the VP rate is monotonic as predicted by the energy gap law, and we conclude that the oscillations are due to Franck–Condon factors that control the EP rate. This relatively simple example of VP/EP competition should be amenable to a detailed theoretical interpretation since the dynamics are not expected to be strongly dependent on the details of the potential.

One interesting question that may be answered by calculations is how the coupling strength depends on the rare gas atom. It seems likely that the coupling will be less for the $HeBr_2$ complex than for $NeBr_2$, and therefore EP will be slower. The EP rate constants for $\nu'=11$ are consistent with this hypothesis, with $NeBr_2$ having an EP rate almost twice as fast as $HeBr_2$. However, for $\nu'=13$, the EP rates are similar. Calculations of the coupling induced by the rare gas atoms should shed light on this strange result.

Previous to this work, a detailed theoretical analysis of the competition between EP and VP has been carried out for ArI_2, $ArCl_2$, and $NeCl_2$.[12–15,20] In the case of ArI_2 the coupling also oscillates over a wide range of vibrational levels, but this is attributed to the IVR-VP dynamics.[13–15] As discussed above, the IVR-VP dynamics are extremely sensitive to the potential, and the case of ArI_2 is not yet well understood. In contrast to ArI_2, the other RgI_2 complexes show simpler dynamics where either VP or EP dominates. In the case of HeI_2 (Ref. 42) and NeI_2 (Ref. 10) only VP is observed, whereas for the Kr (Ref. 17) and Xe (Ref. 17) complexes EP dominates for all ν' levels that have been measured.

Similar to ArI_2, the VP/EP competition for $ArCl_2$ and $NeCl_2$ occurs for levels for which IVR is important and, so far, detailed agreement between experiment and theory has not yet been achieved.[20] In the $RgCl_2$ examples, the 2_g state was identified as the important EP product state.[22] Here we identify the same 2_g state as a possible product EP state for He– and Ne–Br_2. It is interesting to note that for $NeCl_2$ in the T-shaped geometry there is no coupling between the B and 2_g states even though it is symmetry allowed.[22] In the case of the $RgCl_2$ species, it was hypothesized that IVR allows the complex to deviate from the T-shaped symmetry enough to induce the EP coupling. However, for the $RgBr_2$ species it appears that zero-point motion is sufficient to induce coupling. This will be a particularly interesting point to explore in *ab initio* calculations. Also, the analysis of the $RgCl_2$ dynamics indicated that Cl_2 Franck–Condon factors do not control the EP rate in that case.[20] Thus it will be interesting to learn if *ab initio* calculations confirm our conclusion that Franck–Condon factors strongly correlate with EP rate for He– and Ne–Br_2.

As stated above, our conclusion that Franck–Condon factors are important in controlling the EP rates for He– and Ne–Br_2 is supported by the fact that the two species exhibit the same qualitative dependence of the EP rate on ν'. Comparison of the Rg–Br_2 systems to the Rg–Cl_2 systems (each of which has a unique ν' dependence[20]) suggests that the greater spin-orbit coupling in Br_2 is the reason the dynamics are qualitatively different. The greater spin-orbit coupling causes the repulsive potentials to cross the B state at lower ν' and with steeper slopes. The crossing at lower ν' leads to the EP competing with the much simpler direct VP dynamics rather than IVR as in the Rg–Cl_2 complexes. The steeper slopes cause the coupling to occur over a narrow range of halogen nuclear geometries.

Next, we compare the k_{VP} values and the associated direct VP lifetimes extracted from our data to results from previous work. VP lifetimes were obtained for $HeBr_2$ $16 \leq \nu' \leq 38$ by van de Burgt *et al.* from the line broadening of laser excited fluorescence spectra.[43] The lifetimes of the present study are somewhat longer than those of van de Burgt *et al.*, but the differences are not large. However, when Jahn *et al.* measured lifetimes of the $34 \leq \nu' \leq 48$ levels, their values were somewhat larger, and it was suggested that the values of van de Burgt *et al.* were in error by a factor of two.[30] The new results presented here convinced us to reexamine the data reported by van de Burgt *et al.* We used the PGOPHER program[44] and simulated the $20 \leftarrow 0$ rotational contour of Ref. 43 using the experimental parameters also reported in the paper. We found that the lifetime value of the original paper was a much better fit to the data than the larger value suggested by Jahn *et al.*

In a later paper, Jahn *et al.* reported $HeBr_2$ lifetimes for $\nu'=8$, 10 and 12.[41] The values for $\nu'=10$ and 12 are in reasonable agreement with the new values reported here. The Franck–Condon factor we calculated for $\nu'=8$ is large, and as mentioned previously, the lifetime Jahn measured for $\nu'=8$ is 150 ps, much faster than what we predict from our energy gap law fit (256 ps). Therefore, Jahn's results are consistent with our hypothesis that EP to the $1_g/2_g$ state is occurring. Another important result of Ref. 41 is that lifetime broadening is not a function of rotational level but is constant across the whole observed band. This is important in the present study since our broad laser linewidth inherently excites the whole rotational band for each vibrational level.

The VP lifetimes for $HeBr_2$ have been calculated in several theoretical studies, and the agreement with the measured values is quite good, as shown in Table III.[41,45,46] The VP lifetimes listed are from the energy gap law fit shown in Fig. 6. Theoretical studies include golden rule calculations,[41,45] lineshape calculations,[45] and a time-dependent quantum mechanical method.[46] The golden rule and lineshape calculations for higher values of ν' (Ref. 45) are also in excellent agreement with the originally published values of van de Burgt *et al.*[43]

Lifetimes derived from linewidths have been reported for the $\nu'=10$, 14, 16, 17, and 20 levels of $NeBr_2$, and the results are mostly in good agreement with the results presented here.[31] Interestingly, in the previous study results were not obtained for $\nu'=11$ to 13. The authors stated that these levels could not be studied due to spectral congestion.[31] The results here suggest that the signals from these levels were most likely weak in the previous studies due to the competing EP channel. Although the intensities were also weak in the current study and gathering the data presented here required considerable signal averaging, we did not observe any problems with spectral congestion. A more recent study of higher $NeBr_2$ levels by real-time pump-probe spectroscopy similar to that reported here yielded values somewhat larger than the present study.[25] Since that earlier report,

TABLE III. Measured and calculated VP lifetimes for $HeBr_2$. Refs. 45 and 46 used identical Morse potentials (α=1.55 Å^{-1}, D=17 cm^{-1}, and R=3.92 Å) to model the He–Br interaction. Ref. 41 used a Morse potential (α=1.50 Å^{-1}, D=16.07 cm^{-1}, and R=4.022 Å) but switched to a vdW form for the long range part.

	Measured	Calculated			
ν'	τ_{VP} (ps)	τ_{VP} (ps)[a]	τ_{VP} (ps)[b]	τ_{VP} (ps)[c]	τ_{VP} (ps)[d]
10	168 ± 6	140	147	150	146
12	118 ± 3	98	···	106	110
16	62 ± 2	49	···	···	66
20	33 ± 2	28	28	···	41

[a]From golden rule calculation in Ref. 45.
[b]From lineshape calculation in Ref. 45.
[c]From Ref. 46.
[d]From Ref. 41.

we have significantly improved several aspects of our experiment, especially our ability to align the beam through the delay stage. So, we are convinced that the new results are more accurate than those previously reported.

Both classical and quantum mechanical calculations of the $NeBr_2$ VP dynamics have been reported.[32,47,48] A particular focus of the quantum calculations was to characterize the onset of IVR dynamics above $\nu'=20$ as evidenced by non-Lorentzian excitation lineshapes[48] and nonsingle exponential decay of the initially excited state.[32] Below $\nu'=20$, in the direct VP regime, the theoretical results are in good agreement with the VP results from this study (from the energy gap law fit shown in Fig. 6) as reported in Table IV.

IV. CONCLUSIONS

New results for lifetimes of the $HeBr_2$ and $NeBr_2$ B-state vibrational levels are reported and found to have a nonmonotonic dependence on ν'. The deviations from the expected energy gap law behavior are observed for the same ν' levels for each complex and are attributed to an EP process whose rate is controlled by the Franck–Condon factors between the Br_2 B-state vibrational wave functions and the Br–Br product wave functions on the $^3\Pi_g$ (1_g or 2_g) repulsive surface. The 1_g and 2_g surfaces are too similar to be distinguished by this purely experimental study. Since the present data are the first example in which direct vibrational and EP are in competition for a wide range of ν' levels, it presents a particularly attractive case for future theoretical investigation. In other cases for which VP and EP are found to be competitive, the VP occurs in the IVR regime and is thus extremely sensitive to the details of the potential energy surface so that no agreement has been obtained between experiment and theory. IVR will not be an issue in calculations to reproduce the results here.

In addition to future theoretical studies, further experimental results would be particularly useful to help solve the important model problem of competition between vibrational and electronically nonadiabatic dynamics. So far, everything that is known about the $Rg-X_2$ dimers has been inferred from missing X_2 product states and/or nonmonotonic lifetimes for VP. It would be very valuable to monitor EP directly. This could be done by measuring the yield of halogen atom products after excitation of the $Rg-X_2$ complex to the B state. Breen *et al.* have suggested that this could be accomplished by multiphoton ionization-time-of-flight mass spectroscopy, but, to our knowledge, no such experiments have ever been performed.[11] For comparison to theoretical results, a direct measurement of the relative EP/VP quantum yields for a variety of cases would be most valuable. We suggest that He– and $Ne-Br_2$ dimers should be studied first, since they are the only cases for which the EP dynamics have been observed to be in competition with the more easily calculated direct VP dynamics.

TABLE IV. Measured and calculated VP lifetimes for $NeBr_2$. The potential used for the Ne–Br interaction in Refs. 32 and 48 was a Morse potential (α=1.67 Å^{-1}, D=42.0 cm^{-1}, and R=3.90 Å).

	Measured	Calculated	
ν'	τ_{VP} (ps)	τ_{VP} (ps)[a]	τ_{VP} (ps)[b]
10	322 ± 12	394	···
14	120 ± 3	126	···
15	94 ± 3	102	···
16	74 ± 3	71	69.0
17	58 ± 3	61	···
18	45 ± 3	···	39.5
19	35 ± 3	35	48.5
20	28 ± 2	26	27.5

[a]From Ref. 48.
[b]From Ref. 32.

ACKNOWLEDGMENTS

We wish to thank Ramón Hernández-Lamoneda and Craig Bieler for valuable discussions regarding the present results. This research was supported by the National Science Foundation Grant Nos. CHE 0213149 and CHE 0404743. M.A.T. was funded by a Department of Education GAANN fellowship.

[1] R. E. Smalley, D. H. Levy, and L. Wharton, J. Chem. Phys. **64**, 3266 (1976).
[2] A. Rohrbacher, N. Halberstadt, and K. C. Janda, Annu. Rev. Phys. Chem. **51**, 405 (2000).
[3] J. A. Beswick and J. Jortner, Chem. Phys. Lett. **49**, 13 (1977).
[4] J. A. Beswick and J. Jortner, J. Chem. Phys. **69**, 512 (1978).
[5] G. E. Ewing, J. Chem. Phys. **71**, 3143 (1979).

[6] D. D. Evard, C. R. Bieler, J. I. Cline, N. Sivakumar, and K. C. Janda, J. Chem. Phys. **89**, 2829 (1988).
[7] N. Halberstadt, S. Serna, O. Roncero, and K. C. Janda, J. Chem. Phys. **97**, 341 (1992).
[8] G. Kubiak, P. S. H. Fitch, L. Wharton, and D. H. Levy, J. Chem. Phys. **68**, 4477 (1978).
[9] M. L. Burke and W. Klemperer, J. Chem. Phys. **98**, 6642 (1993).
[10] D. M. Willberg, M. Gutmann, J. J. Breen, and A. H. Zewail, J. Chem. Phys. **96**, 198 (1992).
[11] J. J. Breen, D. M. Willberg, M. Gutmann, and A. H. Zewail, J. Chem. Phys. **93**, 9180 (1990).
[12] O. Roncero, N. Halberstadt, and J. A. Beswick, J. Chem. Phys. **104**, 7554 (1996).
[13] O. Roncero and S. K. Gray, J. Chem. Phys. **104**, 4999 (1996).
[14] O. Roncero, A. A. Buchachenko, and B. Lepetit, J. Chem. Phys. **122**, 034303 (2005).
[15] B. Lepetit, O. Roncero, A. A. Buchachenko, and N. Halberstadt, J. Chem. Phys. **116**, 8367 (2002).
[16] A. Burroughs and M. C. Heaven, J. Chem. Phys. **114**, 7027 (2001).
[17] N. Goldstein, T. L. Brack, and G. H. Atkinson, J. Chem. Phys. **85**, 2684 (1986).
[18] J. I. Cline, D. D. Evard, F. Thommen, and K. C. Janda, J. Chem. Phys. **84**, 1165 (1986).
[19] J. I. Cline, B. P. Reid, D. D. Evard, N. Sivakumar, N. Halberstadt, and K. C. Janda, J. Chem. Phys. **89**, 3535 (1988).
[20] C. R. Bieler, K. C. Janda, R. Hernández-Lamoneda, and O. Roncero, J. Phys. Chem. A **114**, 3050 (2010).
[21] J. I. Cline, N. Sivakumar, D. D. Evard, C. R. Bieler, B. P. Reid, N. Halberstadt, S. R. Hair, and K. C. Janda, J. Chem. Phys. **90**, 2605 (1989).
[22] R. Hernández-Lamoneda and K. C. Janda, J. Chem. Phys. **123**, 161102 (2005).
[23] A. Rohrbacher, J. Williams, and K. C. Janda, Phys. Chem. Chem. Phys. **1**, 5263 (1999).
[24] W. E. van der Veer, Laser Focus World **37**, 141 (2001).
[25] J. A. Cabrera, C. R. Bieler, B. C. Olbricht, W. E. van der Veer, and K. C. Janda, J. Chem. Phys. **123**, 054311 (2005).
[26] D. S. Boucher, D. B. Strasfeld, R. A. Loomis, J. M. Herbert, S. E. Ray, and A. B. McCoy, J. Chem. Phys. **123**, 104312 (2005).
[27] J. M. Pio, W. E. van der Veer, C. R. Bieler, and K. C. Janda, J. Chem. Phys. **128**, 134311 (2008).
[28] J. Cabrera, C. R. Bieler, N. McKinney, W. E. van der Veer, J. M. Pio, K. Janda, and O. Roncero, J. Chem. Phys. **127**, 164309 (2007).
[29] M. Nejad-Sattari and T. A. Stephenson, J. Chem. Phys. **106**, 5454 (1997).
[30] D. G. Jahn, S. G. Clement, and K. C. Janda, J. Chem. Phys. **101**, 283 (1994).
[31] J. I. Cline, D. D. Evard, B. P. Reid, N. Sivakumar, F. Thommen, and K. C. Janda, in *Structure and Dynamics of Weakly Bound Molecular Complexes*, edited by A. Weber (Reidel, Dordrecht, 1987) pp. 533–551.
[32] A. García-Vela and K. C. Janda, J. Chem. Phys. **124**, 034305 (2006).
[33] R. F. Barrow, T. C. Clark, J. A. Coxon, and K. K. Yee, J. Mol. Spectrosc. **51**, 428 (1974).
[34] As discussed in Ref. 5, the energy gap, ΔE, is actually the difference between the vibrational frequency of the diatomic, ω_{BrBr}, and the vdW bond energy, D_{RgBr2}. It is only in the limit that $4\pi D_{RgBr2}\omega_{BrBr}/\omega^2_{RgBr2} \gg 1$ that ΔE can be safely approximated by the vibrational spacing of the diatomic.[3] At the request of the reviewer we checked that this approximation was valid for our data by using $\Delta E = \omega_{BrBr} - D_{RgBr2}$ in the fit to see if it changed the VP lifetimes for $NeBr_2$. The resulting values were safely within our error bars, with all the lifetimes but one differing by less than 2%. There was a change of 4.7% for $v' = 20$, which corresponds to a change in lifetime from 27.5 to 26.3 ps.
[35] Although Eq. (4) was derived for a linear complex, it models correctly the behavior for $HeBr_2$ and $NeBr_2$ (see the insets in Figs. 6 and 5). In previous studies it was found that Eq. (4) fits the direct VP dynamics of the T-shaped $HeCl_2$ (Ref. 18) and $NeCl_2$ (Ref. 49) vdW complexes for a range of levels. However, because the complexes in question do not have a linear geometry, information cannot be extracted from the constants A and B.
[36] J. Tellinghuisen, J. Chem. Phys. **115**, 10417 (2001).
[37] J. Tellinghuisen, J. Chem. Phys. **118**, 1573 (2003).
[38] Y. Asano and S. Yabushita, Chem. Phys. Lett. **372**, 348 (2003).
[39] A. Borowski and O. Kühn, Theor. Chem. Acc. **117**, 521 (2007).
[40] D. T. Colbert and W. H. Miller, J. Chem. Phys. **96**, 1982 (1992).
[41] D. G. Jahn, W. S. Barney, J. Cabalo, S. G. Clement, A. Rohrbacher, T. J. Slotterback, J. Williams, K. C. Janda, and N. Halberstadt, J. Chem. Phys. **104**, 3501 (1996).
[42] M. Gutmann, D. M. Willberg, and A. H. Zewail, J. Chem. Phys. **97**, 8037 (1992).
[43] L. J. van de Burgt, J.-P. Nicolai, and M. C. Heaven, J. Chem. Phys. **81**, 5514 (1984).
[44] C. M. Western, PGOPHER, a program for simulating rotational structure, http://pgopher.chm.bris.ac.uk.
[45] T. González-Lezana, M. I. Hernández, G. Delgado-Barrio, A. A. Buchachenko, and P. Villarreal, J. Chem. Phys. **105**, 7454 (1996).
[46] P. J. Krause and D. C. Clary, Chem. Phys. Lett. **271**, 171 (1997).
[47] M. L. González-Martínez, J. Rubayo-Soneira, and K. Janda, Phys. Chem. Chem. Phys. **8**, 4550 (2006).
[48] T. A. Stephenson and N. Halberstadt, J. Chem. Phys. **112**, 2265 (2000).
[49] D. D. Evard, F. Thommen, J. I. Cline, and K. C. Janda, J. Phys. Chem. **91**, 2508 (1987).